



Retrieval of aerosol optical depth from surface solar radiation measurements using machine learning algorithms, nonlinear regression and a radiative transfer based look-up table

J. Huttunen^{1,2}, H. Kokkola¹, T. Mielonen¹, M. Mononen³, A. Lipponen^{1,2}, J. Reunanen⁴, A. V. Lindfors¹, S. Mikkonen², K. E. J. Lehtinen^{1,2}, N. Kouremeti^{5,6}, A. Bais⁶, H. Niska⁷ and A. Arola¹

5 [1]{Finnish Meteorological Institute (FMI), Atmospheric Research Centre of Eastern Finland, Kuopio, Finland.}

[2]{Department of Applied Physics, University of Eastern Finland, Kuopio, Finland.}

[3]{Kuopio, Finland.}

[4]{Tomaattinen Oy, Helsinki, Finland.}

[5] {Physikalisch-Meteorologisches Observatorium Davos, Dorfstrasse 33, CH-7260 Davos Dorf, Switzerland.}

10

[6] {Aristotle University of Thessaloniki, Laboratory of Atmospheric Physics, Thessaloniki, 54124, Greece.}

[7]{Department of Environmental and Biological Sciences, University of Eastern Finland, Kuopio, Finland.}

Corresponding author: J. Huttunen, Finnish Meteorological Institute (FMI), Kuopio Unit, P.O. Box 1627, FI-70211 Kuopio, Finland. (jani.huttunen@fmi.fi)

15 Key points:

- Machine learning methods can produce very good aerosol optical depth estimates from surface solar radiation data
- These tools have the potential to be used to retrieve long aerosol optical depth time series from from surface solar radiation measurements

20

25



Abstract

In order to have a good estimate of the current forcing by anthropogenic aerosols knowledge on past aerosol levels is needed. Aerosol optical depth (AOD) is a good measure for aerosol loading. However, dedicated measurements of AOD are only available from 1990's onward. One option to lengthen the AOD time series beyond 1990's is to retrieve AOD from surface solar radiation (SSR) measurements done with pyranometers. In this work, we have evaluated several inversion methods designed for this task. We compared a look-up table method based on radiative transfer modelling, a nonlinear regression method and four machine learning methods (Gaussian Process, Neural Network, Random Forest and Support Vector Machine) with AOD observations done with a sun photometer at an Aerosol Robotic Network (AERONET) site in Thessaloniki, Greece. Our results show that most of the machine learning methods produce AOD estimates comparable to the look-up table and nonlinear regression methods. All of the applied methods produced AOD values that corresponded well to the AERONET observations with the lowest correlation coefficient value being 0.87 for the Random Forest method. While many of the methods tended to slightly overestimate low AODs and underestimate high AODs, Neural network and support vector machine showed overall better correspondence for the whole AOD range. The differences in producing both ends of the AOD range seem to be caused by differences in the aerosol composition. High AODs were in most cases those with high water vapour content which might affect the aerosol single scattering albedo (SSA) through uptake of water into aerosols. Our study indicates that machine learning methods benefit from the fact that they do not constrain the aerosol SSA in the retrieval where as the LUT method assumes a constant value for it. This would also mean that machine learning methods could have potential in reproducing AOD from SSR even though SSA would have changed during the observation period.

20 1. Introduction

The Fifth Assessment Report of the Intergovernmental Panel on Climate Change states that the most significant source of uncertainty in the projections of climate is related to aerosols (IPCC, 2013). One significant contribution to this uncertainty comes from the fact that without the knowledge of the aerosol burden in the past, we are not able to estimate the current forcing of anthropogenic aerosol. For example, the effect of changes in the current aerosol emissions on climate depends on the background aerosol load during the pre-industrial era (e.g. Andreae, 2007; Carslaw et al., 2013). In addition, the current



estimates of past aerosol emissions are highly uncertain (Granier et al., 2011) thus increased knowledge on historical aerosol levels would increase our ability to estimate the present day aerosol radiative forcing.

One limiting factor in determining the properties of global aerosol in the past has been that observations of aerosol radiative effects have been limited to fairly recent periods. For example, the aerosol optical depth has mainly been measured using sun photometers and the most widely known ground-based network of sun photometers is Aerosol Robotic Network (AERONET; Holben et al., 1998). Although, AERONET contains globally already over 700 stations, with a rather good spatial coverage, it still lacks in temporal coverage, providing aerosol optical properties and AOD only since 1990s, and reaching the current status until the recent years. The earliest records of satellite-based AOD are provided by TOMS (Total Ozone Mapping Spectrometer, e.g. Torres et al., 2002) and AVHRR (Advanced Very High Resolution Radiometer, Geogdzhayev et al., 2005), from 1979 and 1983 onwards, respectively. However, neither one of these instruments were specifically designed to retrieve aerosol properties. The more recent dedicated aerosol sounders, such as ATSR (The Along Track Scanning Radiometer 2, Llewellyn-Jones and Remedios, 2012), MODIS (Moderate Resolution Imaging Spectroradiometer, Levy et al., 2010), VIIRS (Visible Infrared Imaging Radiometer Suite, Jackson et al., 2013), and MISR (Multi-angle Imaging SpectroRadiometer, Kahn and Gaitley, 2015) offer data from 1995, 2000 and 2002 onwards, respectively. It is therefore apparent that neither sun-photometer nor satellite records of AOD extend very far to the past.

There have, however, been recent studies where aerosol load has been indirectly retrieved from surface solar radiation (SSR) measurements, which would cover much longer time periods than sun photometer and satellite observations of AOD. Recently, Kudo et al., 2011 and Lindfors et al., 2013 used SSR measurements done with pyranometers to estimate AOD. Lindfors et al., 2013 demonstrated that AOD can be estimated by using SSR and water vapor information and a look-up table (LUT) generated with a radiative transfer code. Their method produces AOD estimates that have 2/3 of the results within $\pm 20\%$ or ± 0.05 of collocated AERONET AODs. Because pyranometer SSR measurements have been done since 1950's over the globe, the usage of AOD estimates based on SSR measurements would enable us to construct AOD time series that go several decades back in time.



Since the 1990's machine learning methods have made their way to atmospheric sciences and have been used in e.g. satellite data processing, climate modeling, and weather prediction (Hsieh, 2009). Because of their ability to retrieve parameters from data that have strongly non-linear relationships, they have potential of retrieving AOD from a combination of solar radiation measurements and auxiliary data such as water vapour content (WVC) and solar zenith angle (SZA), similarly to what was done by Lindfors et al. (2013) using a radiative transfer based approach. The aim the present work is to investigate how well machine learning methods are able to estimate AOD from pyranometer observations, by evaluating their performance in comparison with a radiative transfer based look-up-table approach. We chose four different methods: Neural Network (NN, McCulloch and Pitts, 1943), Random Forest (RF, Breiman, 2001), Gaussian Process (GP, Santner et al., 2013) and Support Vector Machine (SVM, Smola and Schölkopf, 2004) and compared them against a look-up table and a nonlinear regression method (NR, Bates and Watts, 1988). The performance of these methods was evaluated with AERONET AOD observations done in Thessaloniki, Greece, after the AOD estimates were derived with SSR observations. Nonlinear regression has been successfully used in multiple studies within aerosol and atmospheric sciences (e.g. Huttunen et al., 2014; Ahmad et al., 2013). Out of these machine learning methods, Neural network (NN) has been actively used in different types of applications in atmospheric sciences. For example, it has been applied to retrieve aerosol properties from remote sensing instruments (Olcese et al. 2015; Taylor et al., 2014; Foyo-Moreno et al, 2014). The application of Foyo-Moreno et al. (2014) is similar to ours, in a sense that they also estimated AOD exploiting SSR measurements. In their approach, SSR was separated to direct and diffuse components as inputs for NN to estimate AOD. To our knowledge, the rest of the analyzed methods have not been used to retrieve aerosol properties directly from observations.

2. Data and Methods

We compared the ability of several methods to estimate AOD, based on SSR and water vapor measurements (and SZA that can be readily determined for any given time and location), against AERONET AOD measurements at 500 nm (henceforth AOD) done at Thessalonki, Greece. This site was chosen for this study, because it has all the necessary measurements with high quality from a 10 year time period, and because it is the same site to which Lindfors et al. (2013) applied their LUT-approach. Furthermore, the location has varying aerosol concentrations and relatively high AOD values throughout the year.



2.1 Pyranometer measurements of surface solar radiation

SSR has been measured at Thessaloniki since January 1993 with a CM21 pyranometer manufactured by Kipp and Zonen. The instrument is located on the roof of the Physics Department at the Aristotle University of Thessaloniki (40.63 N, 22.96 E), ca. 60 m above sea level. The data are sampled every 1–2 s and every minute the average and standard deviation of the samples are recorded (see more details from Lindfors et al., 2013). The calibration of the pyranometer has been confirmed to stay within the quoted by the manufacturer accuracy (Bais et al., 2013).

2.2 AERONET measurements

AERONET is a network of sun and sky scanning radiometers that measure direct sun and sky radiance at several wavelengths, typically centered at 340, 380, 440, 500, 670, 870, 940, and 1020 nm, providing measurements of various aerosol related properties (Holben et al., 1998). From direct sun measurements we exploited AOD and WVC data. When also sky radiance measurements are included, more detailed aerosol properties such as single scattering albedo (SSA) and asymmetry parameter (g) can be retrieved (Dubovik et al., 2000). In the evaluation of the machine learning methods we used Level 2.0 (cloud-screened and quality assured) AERONET direct sun measurements of AOD and WVC for Thessaloniki. The Cimel sun photometer is located at the roof of the Physics Department in the close vicinity of the pyranometer discussed above. From the inversion products, to interpret some of our results in more detail, we used level 1.5 (cloud-screened) retrievals. However, when we selected the data from the Level 1.5 inversion product, we applied all the other level 2.0 AERONET criteria except for the AOD threshold. In other words, we applied otherwise the same rigorous quality control that is required for Level 2 data, but we only relaxed the requirement for AOD at 440nm to range from 0.4 to 0.1, in order to have more reliable measurements for our data analysis.

2.3 Cloud-screening of the pyranometer measurements and collocation with the AERONET measurements

Cloud-screening is a crucial factor in the analysis, thus only contribution of aerosols are considered, not clouds. The cloud-screening was first applied to the SSR data and only the clear-sky measurements were included in the analysis (see Lindfors



et al., 2013 for more details). After the initial cloud-screening, the SSR data still included observations with corresponding AOD values that deviated significantly from the main body of the observations. Since there is a high probability that these outliers in the data were caused by e.g. cloud-contamination, we applied additional screening to the data. Thus, we removed the clear outliers of possibly undetected clouds, in our case those observations that deviated by more than $\pm 20 \text{ Wm}^{-2}$ from the exponential regression fit ($\text{SSR} = a \cdot \exp(-b \cdot \text{AOD}) + c$, where a , b and c are regression constants). This additional screening was applied through regression of SSR against AOD for a given range of SZA (within $\pm 0.5^\circ$). The the SSR values were collocated for each AOD with the ± 1 minutes difference, averaged and finally normalized for the Sun-Earth distance corresponding to January 1st. The training dataset for the machine learning methods contained years 2009-2014 and the validation (verification) dataset years 2005-2008. These periods were selected because we wanted to verify if the methods could provide reasonable AOD estimates for a period different than the training. The training dataset covered approximately 2/3 and the validation dataset 1/3 of the whole data. For all the methods the input parameters are SSR, WVC and SZA, and they produce AOD estimates.

2.4 LUT and NR methods for AOD retrievals

2.4.1 Radiative transfer model based look-up table (LUT)

To retrieve AOD from SSR observations Lindfors et al., (2013) produced a LUT based on radiative transfer simulations. They simulated SSR in different atmospheric conditions by varying AOD, WVC and SZA systematically. They used a single aerosol model for all the simulations, and therefore called their AOD estimate as an effective AOD, which is only a function of SSR, SZA, WVC. Other parameters were assumed as constants e.g. Ångström Exponent of 1.1, SSA at 500 nm of 0.92 (the SSA's spectral pattern follows the rural background aerosol model by Shettle, 1989, where SSA changes from roughly 0.92 at 400 nm to 0.89 at 1000 nm), the asymmetry parameter was assumed wavelength independent with a value of 0.68 while the albedo was varying with wavelength and SZA. For a more detailed description of the LUT method see Lindfors et al., (2013).

2.4.2 Nonlinear regression method (NR)



The nonlinear regression (NR) is a multivariate analysis method which is used when the dependencies between the study variables are not linear (Bates and Watts, 1988). NR is useful especially when there are physical reasons for believing that the relationship between the response and the predictors follows a particular functional form. Benefits of NR are that it needs only moderate sized sample of the studied phenomena to give adequately precise results and as an output it gives a simple, but not predefined, function for prediction. Additional advantage of NR against the other methods presented in this paper is that once the parameters are estimated, they can be used in similar cases without additional training data. In this study we assume that AOD can be estimated as a function of SSR, WVC and SZA. Multiple different formulations for the NR function was tested and the function with the best prediction ability found for this data is given by

$$\text{AOD} = b_0 + b_1 \exp(1/\text{sza}) + b_2 \exp(1/\text{flux}) + b_3 \exp(1/\text{wvc}) + b_4 \exp(1/\text{sza}) \exp(1/\text{flux}) + b_5 \exp(1/\text{sza}) \exp(1/\text{wvc}) + b_6 \exp(1/\text{flux}) \exp(1/\text{wvc}).$$

The coefficients b_0 - b_6 were determined using R-software (R Core Team, 2014).

2.5 Machine learning methods for AOD retrievals

2.5.1 Neural Network (NN)

Artificial neural networks (NN) belong to the family of machine learning methods (McCulloch and Pitts, 1943). As usually in machine learning methods, the aim of an artificial neural network is to generate a mathematical model to represent the phenomenon that is examined. The mathematical model of NN structure specifically consists of interconnected neurons with numeric weights. A typical NN model is multilayer perceptron (MLP) (Rosenblatt, 1958), which is used in this study. A MLP network consists of several neuron layers: an input layer, hidden layers and an output layer. The weights and other parameters of the model are tuned or trained with a specific training set containing input-output pairs of the phenomenon. In this case the inputs are SSR, WVC, SZA and the output is AOD. The training is executed with a training algorithm, in this paper the Levenberg-Marquardt algorithm is used (Hagan and Menhaj, 1994). A total of 20 neural networks were trained in this case. Each network had its own number of neurons in a hidden layer. The networks which learned the training set best



were selected to a group which contained five networks. The final estimate of networks was given as a median of the outputs of all members of the group.

2.5.2 Random Forest (RF)

Random Forest (RF) (Breiman, 2001) is a machine learning technique that is used for classification and nonlinear regression.

5 RF for nonlinear regression consists of an ensemble of binary regression trees. Each of these trees is constructed using a randomized training scheme and is essentially a piecewise constant fit to the training data set. The prediction of a RF model is obtained by averaging the regression tree predictions over the whole ensemble. In this study, the RF implementation from the Scikit-Learn machine learning library (Pedregosa et al. 2011) was used. The RF model inputs were (SSR, WVC, SZA, SSR*WVC, SSW*SZA, WVC*SZA) and the output (AOD). A randomized cross-validation scheme was used to find the
10 optimal training parameters for the RF: $\text{min_samples_split} = 4$, $\text{max_features} = 1.0$, $\text{min_samples_leaf} = 2$, $\text{n_estimators} = 225$, $\text{max_depth} = 39$. For more information on RFs see, for example, Friedman et al., (2001).

2.5.3 Support vector machine (SVM)

Support vector machine (SVM) is a novel machine learning technique (Vapnik, 1995; Burges, 1998), which has many benefits to the conventional artificial-NNs (Haykin, 1999). In this study, we use the standard SVM regression (SVR), the
15 formulation based on the commonly used ϵ -SVR with radial basis kernel function (implemented in the libsvm package). The objective of ϵ -SVR is to find a function that has at most ϵ deviation from the actual outputs for all the training data and is at the same time as flat as possible. The proposed modelling problem can be formulated as a quadratic (convex) optimization problem based on minimization of the Vapnik's ϵ -insensitive loss function (e.g. Vapnik 1995). In principle, there are two parameters to be controlled: the regularization parameter, which controls the smoothness of the approximation function
20 (sensitivity to noise), and the parameter ϵ , which dominates the number of support vectors by governing the accuracy of the approximation function. The determination of SVM control parameters was solved by means of a grid search. For a more detailed description of the method, the reader is referred e.g. to Smola and Schölkopf (2004).

2.5.4 Gaussian process (GP)



Gaussian process (GP) for machine learning is a generic supervised learning method that may be used, for example, for nonlinear regression. In GP learning, the function inputs and outputs are treated as Gaussian random variables and the correlations between these variables are modelled. The predictions given by a GP model are computed as conditional probability distributions given the training data and function inputs. As the GP predictions are probability distributions, the error estimates for the predicted point estimates are obtained automatically. In this study, the GP implementation from the Scikit-Learn machine learning library was used. The same inputs and output variables as with the RF model were used in the GP training. A total of 25 GP models were trained. The training of each model was carried out using 2500 training data samples that were randomly sampled from the full training data set. A squared exponential autocorrelation function and the following training parameters were used in the training: $\theta_0 = 1.0e-8$, $\theta_L = 1.0e-16$, $\theta_U = 1.0$, $\text{nugget} = 1.0e-3$. The five best performing GP models were selected into the final GP model committee. The final prediction was computed as the median of the predictions given by the GP models in the committee. For more information on GPs for machine learning see, for example, Welch et al., (1992), Rasmussen and Williams (2006), and Santner et al., (2013).

3. Results

3.1 Comparison of the methods

Table 1 shows the statistics of the AOD observed by AERONET together with the statistical characteristics of the predicted AOD for the years 2005-2008. From the table, we can see that predicted values show good correlation against the observations for all the methods. Predictions by RF had the lowest correlation coefficient with a value of 0.87 while the correlation coefficient for NR was only slightly larger, 0.88. For the best performing methods, LUT, GP, NN, and SVM, the correlation coefficients were approximately 0.92. Their predicted AODs in comparison to AERONET AOD are shown in Figure 1. Based on the different statistics in Table 1, machine learning methods (NN, SVM, GP) produce a good match with AERONET data and they perform equally good or better than the LUT method according to all the metrics. Due to the fact that RF and NR are not able to produce as good estimates as the LUT method, they were left out from the more detailed analysis.



Although these methods are able to predict the average AOD with a good accuracy, they differ when we compare their ability to predict different AOD levels. In Figure 1, the color scales indicate the absolute amount of results in the areas with the interval of 0.01×0.01 (vertically and horizontally) for AOD, in addition 1:1-lines and linear fits are included. Based on the linear fits, NN appears to have the best agreement with AERONET data for the whole AOD range. As the average and median values of AERONET AOD are 0.240 and 0.207 respectively (Table 1), the main population of the measurements is in the range of moderate AODs. The machine learning methods are obviously weighted to perform best in this range of AODs. However, from Figure 2, which shows the absolute difference between AERONET and predicted AOD, we can see that LUT and GP tend to significantly underestimate AOD for AODs larger than 0.5, while NN and SVM are able to reach smaller differences with AERONET on average, although with larger overall variabilities than LUT and GP. Although NN and SVM also start to deviate from the observations at higher AODs, these deviations are more modest in relative sense as can be seen from Figure 3 which shows the relative difference between the observations and predictions. All the methods overestimate AOD in relative terms, when AOD approaches zero (Figure 3). However, as Figure 2 demonstrates, the absolute error is systematically very low in the small AOD region ($AOD < 0.2$). NN and SVM are generalized better for large AODs than the other methods, where the amount of data are small.

15 3.2 The effect of water vapour on AOD predictions

Huttunen et al. (2014) showed that WVC and AOD have typically a positive correlation. Therefore, we investigated how the AOD estimates from different methods are affected by WVC. Figure 4 shows the relative difference between the predictions and measured AOD with respect to WVC. From this figure, we can see that the LUT-based AODs are overestimated at the smallest and underestimated at the largest WVC contents. The reason for this behaviour is that the LUT method has been set to assume prescribed and constant properties for many relevant parameters that affect SSR (other than AOD and WVC); e.g. aerosol single scattering albedo, asymmetry parameter and surface albedo (Lindfors et al., 2013). Consequently, the assumption of constant SSA in particular leads to WVC-dependent systematic bias of the LUT-based AOD, as we will show next. The other methods are closer to the ratio of 1 without such a systematic bias, excluding the SVM's underestimation for the smallest WVC.



Figure 5 shows measured SSR and LUT-based SSR for a narrow set of SZAs (49.75° - 50.25°). AOD is on the horizontal axis, SSR on the vertical axis and WVC is shown with the colorbar. From Figure 5a it is evident that LUT incorporates a strong WVC-dependent structure: for a given SSR level, AOD decreases with increasing water vapor content. This pattern follows from the assumption that the aerosol composition remains the same, i.e. it has a fixed SSA value. Thus in the LUT method, increases in SSR absorption by water vapour are compensated by decreases in aerosol extinction. In the real atmosphere, water vapour content has also implications on aerosol composition and size. If all conditions apart from water vapour remained constant, increase of water vapour would also increase the uptake of water into aerosol particles thus affecting the aerosol SSA. The effect of fixed SSA is also visible in the way the LUT-based AOD estimates are distributed (Figure 5a). In Figure 5c we can see that for a given AOD in the LUT, the highest WVC values always correspond to the lowest SSR values. However, the same pattern is not clearly visible either in the plot with the measured values (Figure 5b) or in the plot with AOD from NN (Figure 5d). This indicates that although the machine learning methods do not get explicitly any information about the possible systematic co-variability of WVC and SSA, they seem to be able to detect it indirectly, at least to some extent.

To further illustrate this, Figure 6a shows the AERONET measurements of AOD and single scattering co-albedo, 1-SSA at 670 nm as a function of WVC. Here, together with the absorption strength by the water vapour, we considered more illustrative to show the single scattering co-albedo rather than SSA. In this plot, SZA, SSR and season were limited respectively to: $58^{\circ} < \text{SZA} < 62^{\circ}$, $420 \text{ Wm}^{-2} < \text{SSR} < 460 \text{ Wm}^{-2}$, June-August, allowing enough data with the limited parameters. Thus, the plot illustrates the co-variability of WVC and SSA for a limited range of surface solar radiation and SZA, for conditions when the LUT method produces lower AOD values for higher WVC (Figure 5a). However, Figure 6a clearly shows that an opposite relationship between AOD and WVC is obtained by the measurements. Moreover, this pattern is compensated by aerosol absorption (remember that in this sub-set we constrained SSR), which decreases with increasing WVC; this is likely related to the aerosol swelling by hygroscopic growth that increases the scattering of the aerosol. Therefore, we can conclude from the measurements that because of the co-variability of WVC and SSA in Thessaloniki, the assumption of a fixed SSA in the LUT causes limitations for predicting AOD, while the machine learning methods can take into account, at least to some extent, this relationship indirectly. Using radiative transfer modeling we demonstrated that the



magnitude of these changes in water vapor and aerosol absorption, as indicated in Figure 6. Indeed, they induced opposite effects of similar magnitude in surface solar irradiance. For the base case, we simulated SSR with WVC of 2.8 cm and 1-SSA of 0.06 (with SZA of 60° and AOD of 0.3) as inputs, resulting in 439.9 Wm⁻². When we increased the water vapour column to 3.6 cm, the corresponding decrease in SSR was about 6.8 Wm⁻². However, when we additionally decreased the aerosol absorption (1-SSA) to 0.04, the difference to the base case shrank to 1.8 Wm⁻² and this remaining amount can mostly be explained by the asymmetry parameter, which also exhibits a systematic dependence with WVC (stronger forward scattering by particles grown in humid conditions).

The lower panel of Figure 6 further illustrates the role of fixed SSA in the observed WVC-dependent bias in the LUT results, which can be avoided with the machine learning methods. It shows the mean ratio of LUT-estimated and AERONET-measured AOD on the right-hand side y-axis as a function of water vapour content (so essentially the same results shown by a box-plot in Figure 4). Additionally, on the left-hand side y-axis, the single scattering albedo (estimated for 500 nm) from AERONET measurements is shown as a function of water vapour amount as well. This also demonstrates that the over- and underestimations of the LUT method coincide with SSA range that is under and over the assumed fixed value of 0.92 (shown with red dashed line), respectively. Visibly, the ratio in the right-hand axis of Fig. 6b, reaches one not until SSA is roughly 0.93 instead of 0.92. Presumably, SSA has actually a different wavelength pattern than the one assumed in LUT.

4. Conclusions

We have used several inverse methods to retrieve aerosol optical depth (AOD) from surface solar radiation (SSR) and water vapour content (WVC) measurements (with corresponding solar zenith angle data) done in Thessaloniki, Greece. Two traditional (look-up table (LUT) and nonlinear regression (NR)) and four machine learning methods (Gaussian Process (GP), Neural Network (NN), Random Forest (RF) and Support Vector Machine (SVM)) were used to retrieve AOD estimates for the years 2005-2008. Then we compared the AOD estimates with collocated AOD measurements done by Aerosol Robotic Network (AERONET). Our comparisons showed that:

- AOD estimates based on the LUT method agreed better with AERONET than the NR estimates but apart from RF, the machine learning methods produced AOD estimates that were comparable or better than LUT.



- NN and SVM methods reproduced good correspondence to AERONET observations for both low and high AODs while rest of the methods tended to overestimate low AODs and underestimate high AODs. The main reason for the better performance of these machine learning methods was that there were no constraints of the aerosol single scattering albedo (SSA) in the retrieval. In other words, the methods do not need to explicitly make assumptions on the optical aerosol properties of the atmosphere and because seem to be able to indirectly account for the covariation of WVC and SSA.
- When compared with AERONET measurements, the best AOD estimates were retrieved with the machine learning algorithms, but only NN and SVM were able to generalize accurate estimates also for large AODs.
- The machine learning methods are sensitive to the selection of the training data set and other constraints, and are generally valid only for the range of the variables used for their training; thus care needs to be taken when these methods are employed.
- These tools have the potential to be used in the retrieval of AOD from SSR measurements to lengthen the time series of AOD. Historical AOD is essential in the estimation of anthropogenic aerosol effects and in the evaluation of AOD retrievals from space borne instruments before the 1990s.

Acknowledgements.

- We thank the AERONET team, principal investigators and other participants for their effort in establishing and maintaining the network. This study is supported by Graduate school in Physics, Chemistry, Biology and Meteorology of Atmospheric Composition and Climate Change: From Molecular Processes to Global Observations and Models. The Academy of Finland Center of Excellence program (project number 272041) is also acknowledged. The financial support by the strategic funding of the University of Eastern Finland is gratefully acknowledged. The author thank Juha Tonttila and Mikko Pitkänen from Finnish Meteorological Institute, Kuopio, for their help with the python (python.org) and in the production of the MatLab (mathworks.com) boxplot-figures. Also JH thank the Finnish Cultural Foundation, North Savo Regional fund.

References

Ahmad, I., Mielonen, T., Grosvenor, D., Portin, H., Arola, A., Mikkonen, S., Kühn, T., Leskinen, A., Joutsensaari, J., Komppula, M., Lehtinen, K., Laaksonen, A. and Romakkaniemi, S. (2013). Long-term measurements of cloud droplet



- concentrations and aerosol-cloud interactions in continental boundary layer clouds. *Tellus B*, 65. doi:<http://dx.doi.org/10.3402/tellusb.v65i0.20138>.
- Andreae, M. O. and Rosenfeld, D. Aerosol–cloud–precipitation interactions. Part 1. The nature and sources of cloud-active aerosols. *Earth Sci. Rev.* 89, 13–41, 2008.
- 5 Bais, A. F., Drosoglou, Th., Meleti, C., Tourpali, K. and Kouremeti, N., Changes in surface shortwave solar irradiance from 1993 to 2011 at Thessaloniki (Greece). *Int. J. Climatol.*, 33: 2871–2876. doi: 10.1002/joc.3636, 2013.
- Bates D.M. and Watts D. G., *Nonlinear Regression Analysis and Its Applications*, Wiley, New York, 1988.
- Breiman, L., *Random forests*, *Machine learning*, vol 45, 1, 5-32, 2001.
- Burges C. J. C., A tutorial on support vector machines for pattern recognition, *Data Mining and Knowledge Discovery*, 2,
10 121–167, 1998.
- Carslaw K. S., Lee L. A., Reddington C. L., Pringle K. J., Rap A., Forster P. M., Mann G. W., Spracklen D. V., Woodhouse M. T., Regayre L. A. and Pierce J. R., Large contribution of natural aerosols to uncertainty in indirect forcing, *Nature*, 2013.
- Dubovik, O., A. Smirnov, B. N. Holben, M. D. King, Y.J. Kaufman, T. F. Eck, and I. Slutsker, 2000: Accuracy assessments of aerosol optical properties retrieved from AERONET sun and sky-radiance measurements, *J. Geophys. Res.*, 105, 9791-9806.
- 15 Foyo-Moreno I., Alados I., Anton M., Fernandez-Galvez J., Cazorla A. and Alados-Arbodelas L., Estimating aerosol characteristics from solar irradiance measurements at an urban location in southeastern Spain, *J. of Geophys. Res. Atmos*, 119, 1845-1859, doi:10.1002/2013JD020599, 2014.
- Friedman J., Hastie T., and Tibshirani R., *The elements of statistical learning*, Springer, vol 1, 2001.
- Geogdzhayev, I. V., M. I. Mishchenko, E. I. Terez, G. A. Terez, and G. K. Gushchin, Regional advanced very high resolution radiometer–derived climatology of aerosol optical thickness and size, *J. Geophys. Res.*, 110, D23205, doi:10.1029/2005JD006170, 2005.
- 20 Claire Granier, Bertrand Bessagnet, Tami Bond, Ariela D’Angiola, Hugo Denier van der Gon, Gregory J. Frost, Angelika Heil, Johannes W. Kaiser, Stefan Kinne, Zbigniew Klimont, Silvia Kloster, Jean-François Lamarque, Catherine Liousse, Toshihiko Masui, Frederik Meleux, Aude Mieville, Toshimasa Ohara, Jean-Christophe Raut, Keywan Riahi, Martin G.
- 25 Schultz, Steven J. Smith, Allison Thompson, John van Aardenne, Guido R. van der Werf, and Detlef P. van Vuuren, Evolution of anthropogenic and biomass burning emissions of air pollutants at global and regional scales during the 1980–2010 period, *Climatic Change*, 109, 1, 163-190, 2011.
- Hagan M.T. and Menhaj M.B., Training feedforward networks with the Marquardt algorithm, *IEEE Trans. Neural Networks*, 5, 6, 989-993, 1994.



- Haykin S., *Neural Networks: A Comprehensive Foundation*. 2nd Edition. NJ: Prentice-Hall, 1999.
- Holben B.N., T.F. Eck, I. Slutsker, D. Tanre, J.P. Buis, A. Setzer, E. Vermote, J.A. Reagan, Y. Kaufman, T. Nakajima, F. Lavenu, I. Jankowiak, and A. Smirnov, 1998: AERONET - A federated instrument network and data archive for aerosol characterization, *Rem. Sens. Environ.*, 66, 1-16.
- 5 Hsieh, *Machine Learning Methods in the Environmental Sciences Neural Networks and Kernels*, Cambridge Univ Press, 2009.
- Huttunen, J., Arola, A., Myhre, G., Lindfors, A. V., Mielonen, T., Mikkonen, S., Schafer, J. S., Tripathi, S. N., Wild, M., Komppula, M., and Lehtinen, K. E. J.: Effect of water vapor on the determination of aerosol direct radiative effect based on the AERONET fluxes, *Atmos. Chem. Phys.*, 14, 6103-6110, doi:10.5194/acp-14-6103-2014, 2014.
- 10 IPCC, *Climate Change 2013: The Physical Science Basis*. Contribution of Working Group I to the Fifth Assessment Report of Intergovernmental Panel on Climate Change, Cambridge University Press, Cambridge, United Kingdom and New York, NY, USA, ISBN 978-1-107-66182-0, doi:10.1017/CBO9781107415324, 2013.
- Jackson, J. M., H. Liu, I. Laszlo, S. Kondragunta, L. A. Remer, J. Huang, and H.-C. Huang, Suomi-NPP VIIRS aerosol algorithms and data products, *J. Geophys. Res. Atmos.*, 118, 12,673–12,689, doi:[10.1002/2013JD020449](https://doi.org/10.1002/2013JD020449), 2013.
- 15 Kahn, R. A., and B. J. Gaitley, An analysis of global aerosol type as retrieved by MISR. *J. Geophys. Res. Atmos.*, 120, 4248–4281. doi: [10.1002/2015JD023322](https://doi.org/10.1002/2015JD023322), 2015.
- Kudo, R., Uchiyama, A., Yamazaki, A., Sakami, T., and Ijima, O., Decadal changes in aerosol optical thickness and single scattering albedo estimated from ground-based broadband radiometers: A case study in Japan, *J. Geophys. Res.*, 116, D03207, doi:10.1029/2010JD014911, 2011.
- 20 Levy, R. C., Remer, L. A., Kleidman, R. G., Mattoo, S., Ichoku, C., Kahn, R., and Eck, T.F., Global evaluation of the Collection 5 MODIS dark-target aerosol products over land, *Atmos. Chem. Phys.*, 10, 10399-10420, doi:10.5194/acp-10-10399-2010, 2010.
- Llewellyn-Jones D. and Remedios J., The Advanced Along Track Scanning Radiometer (AATSR) and its predecessors ATSR-1 and ATSR-2: An introduction to the special issue, *Remote Sensing of Environment*, Vol 116, 15, Pages 1–3, doi:10.1016/j.rse.2011.06.002, 2012.
- 25 Lindfors, A. V., Kouremeti, N., Arola, A., Kazadzis, S., Bais, A. F., and Laaksonen, A., Effective aerosol optical depth from pyranometer measurements of surface solar radiation (global radiation) at Thessaloniki, Greece, *Atmos. Chem. Phys.*, 13, 3733-3741, doi:10.5194/acp-13-3733-2013, 2013.
- McCulloch, W. and Pitts W., A Logical Calculus of Ideas Immanent in Nervous Activity, *Bulletin of Mathematical Biophysics* 5, 4, 115–133. doi:10.1007/BF02478259, 1943.
- 30



- Olcese L. E., Palancar G. G. and Toselli B. M., A method to estimate missing AERONET AOD values based on artificial neural networks, *Atmospheric Environment*, 113, 140–150, doi:10.1016/j.atmosenv.2015.05.009, 2015.
- Pedregosa, F., Varoquaux, G., Gramfort, A., Michel, V., Thirion, B., Grisel, O., Blondel, M., Prettenhofer, P., Weiss, R., Dubourg, V., Vanderplas, J., Passos, A., Cournapeau, D., Brucher, M., Perrot, M., and Duchesnay, E., Scikit-learn: Machine
5 Learning in Python, *Journal of Machine Learning Research*, 12, 2825-2830, 2011.
- R Core Team (2014). R: A language and environment for statistical computing. R Foundation for Statistical Computing, Vienna, Austria. URL <http://www.R-project.org/>.
- Rasmussen, C.E. and Williams, C.K.I., *Gaussian processes for machine learning*, MIT Press, 2006.
- Santner, T. J., Williams, B. J., and Notz, W. I., *The design and analysis of computer experiments*, Springer Science &
10 Business Media, 2013.
- Rosenblatt, F. A., probabilistic model for information storage and organization in the brain, *Psychol. Rev.*, 65, 6, 368-408, 1958.
- Shettle, E. P., Models of aerosols, clouds and precipitation for atmospheric propagation studies, in: *Atmospheric Propagation in the UV, Visible, IR and mm-region and Related System Aspects*, no. 454 in AGARD Conf. Proc., 15–1–15–13, 1989.
- 15 Smola A. J. and Schölkopf B., A tutorial on support vector regression, *Stat. Comput.*, 14, 199-222, 2004.
- Taylor, M., Kazadzis, S., Tsekeri, A., Gkikas, A., and Amiridis, V., Satellite retrieval of aerosol microphysical and optical parameters using neural networks: a new methodology applied to the Sahara desert dust peak, *Atmos. Meas. Tech.*, 7, 3151-3175, doi:10.5194/amt-7-3151-2014, 2014.
- Torres, O., Bhartia P. K., Herman J. R., Sinyuk A., Ginoux P., and Holben B., A long-term record of aerosol optical depth
20 from TOMS observations and comparison to AERONET measurements, *Journal of the Atmospheric Sciences*, 59, 3, 398-413, 2002.
- Vapnik, V., *The Nature of Statistical Learning Theory*. New York: Springer, 1995.
- Welch, W. J., Buck, R. J., Sacks, J., Wynn, H. P., Mitchell, T. J., and Morris, M. D., Screening, predicting, and computer experiments, *Technometrics*, vol 34, 1, 15-25, 1992.
25

Table 1: Statistical characteristics of observed (AERONET) and predicted AOD by the methods of NR (nonlinear regression), LUT (look-up table), NN (neural network), RF (random forest), GP (gaussian process), SVM (support vector machine) and some of their combinations (averages without weights). Correlation coefficient (R^2), mean absolute deviation



(MAD), median and their $\pm 20\%$ percentiles between the observed and predicted. Also time consumptions with a recent average computer power of the methods for training / estimation in the magnitude of seconds, minutes and hours. The number of observations is 10684.

| Method | Average(std) | R ² | MAD | Median | Fraction in +/- 20% | Time consumption |
|-------------|---------------------|----------------|-------|--------------|---------------------|----------------------------|
| AERONET | 0.240(0.147) | | | 0.207 | | |
| NR | 0.228(0.123) | 0.880 | 0.053 | 0.210 | 48.4 % | seconds / < second |
| LUT | 0.254(0.136) | 0.920 | 0.046 | 0.236 | 52.6 % | hours / minutes |
| NN | 0.251(0.156) | 0.920 | 0.044 | 0.212 | 59.1 % | hours / < second |
| RF | 0.225(0.116) | 0.870 | 0.052 | 0.204 | 52.9 % | tens of seconds / < second |
| GP | 0.240(0.130) | 0.927 | 0.041 | 0.213 | 60.8 % | minutes / tens of seconds |
| SVM | 0.242(0.150) | 0.918 | 0.044 | 0.201 | 58.4 % | tens of seconds / < second |
| NN, SVM | 0.247(0.152) | 0.924 | 0.043 | 0.207 | 59.7 % | |
| NN, SVM, RF | 0.240(0.138) | 0.922 | 0.042 | 0.205 | 59.9 % | |
| SVM, RF | 0.234(0.131) | 0.913 | 0.044 | 0.202 | 58.0 % | |
| NN, RF | 0.238(0.134) | 0.916 | 0.043 | 0.207 | 59.0 % | |

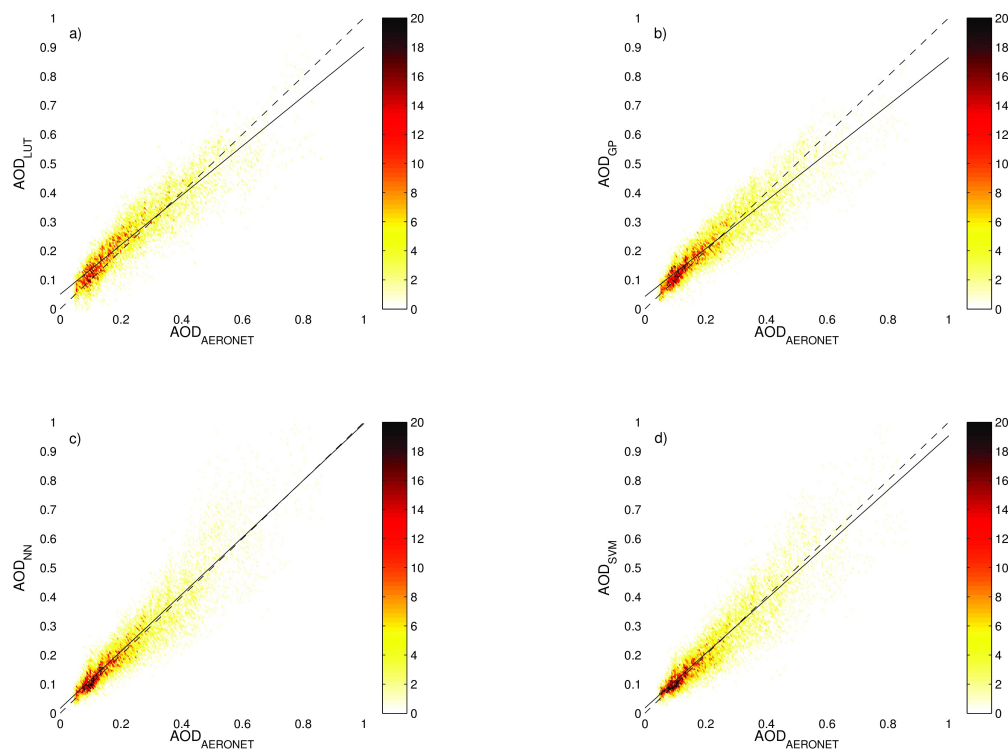


Figure 1: Observed (AERONET) and predicted AOD by the methods of a) LUT (look-up table), b) GP (Gaussian Process), c) NN (Neural Network) and d) SVM (Support Vector Machine). The colorbar indicates the absolute amount of results in the areas with the interval of 0.01×0.01 . The 1:1-lines and linear fits included. The number of observations is 10684.

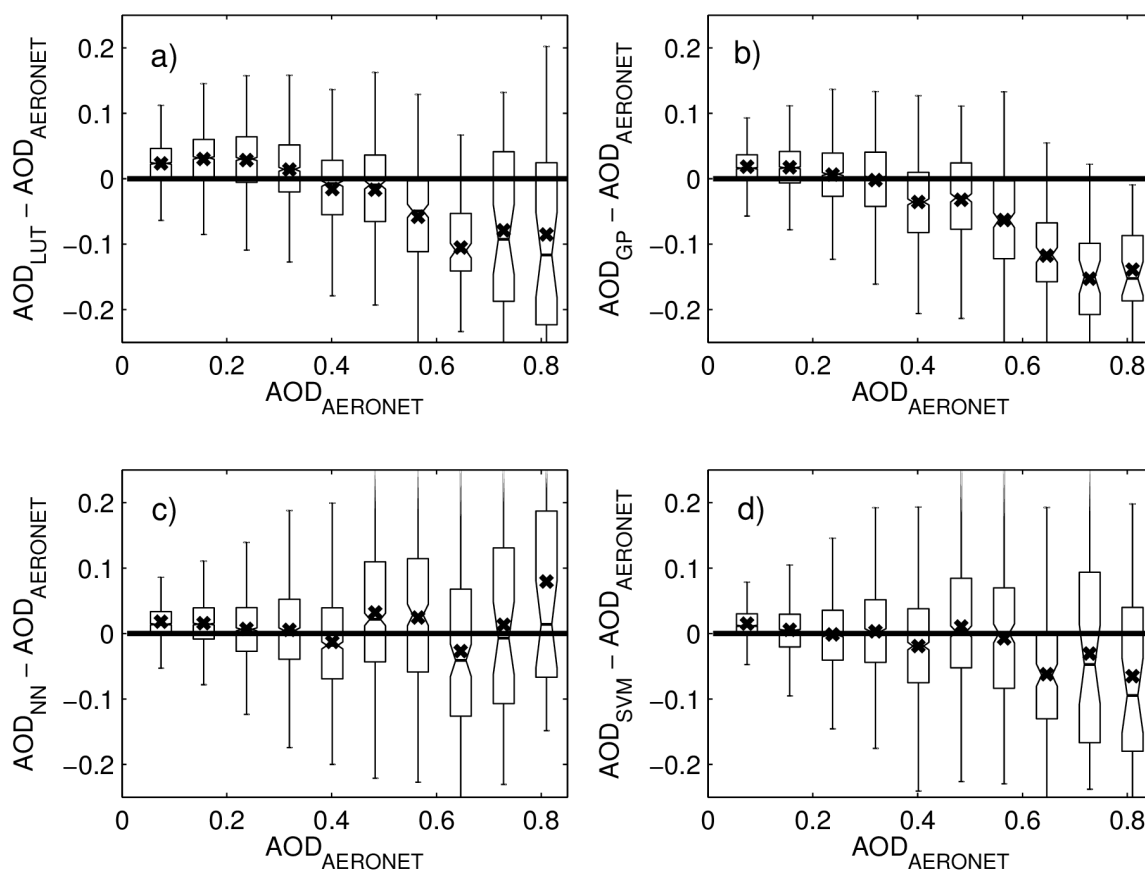


Figure 2: Differences between predicted and observed (AERONET) AOD for the methods: a) LUT (look-up table), b) GP (Gaussian Process), c) NN (Neural Network) and d) SVM (Support Vector Machine) with respect of the observed AOD. The crosses indicate the means of each sub-group, the limits of the boxes are 25 %, 50 % and 75 % of the data, and the lines are plotted with 1.5 times the inter-quartile ranges.

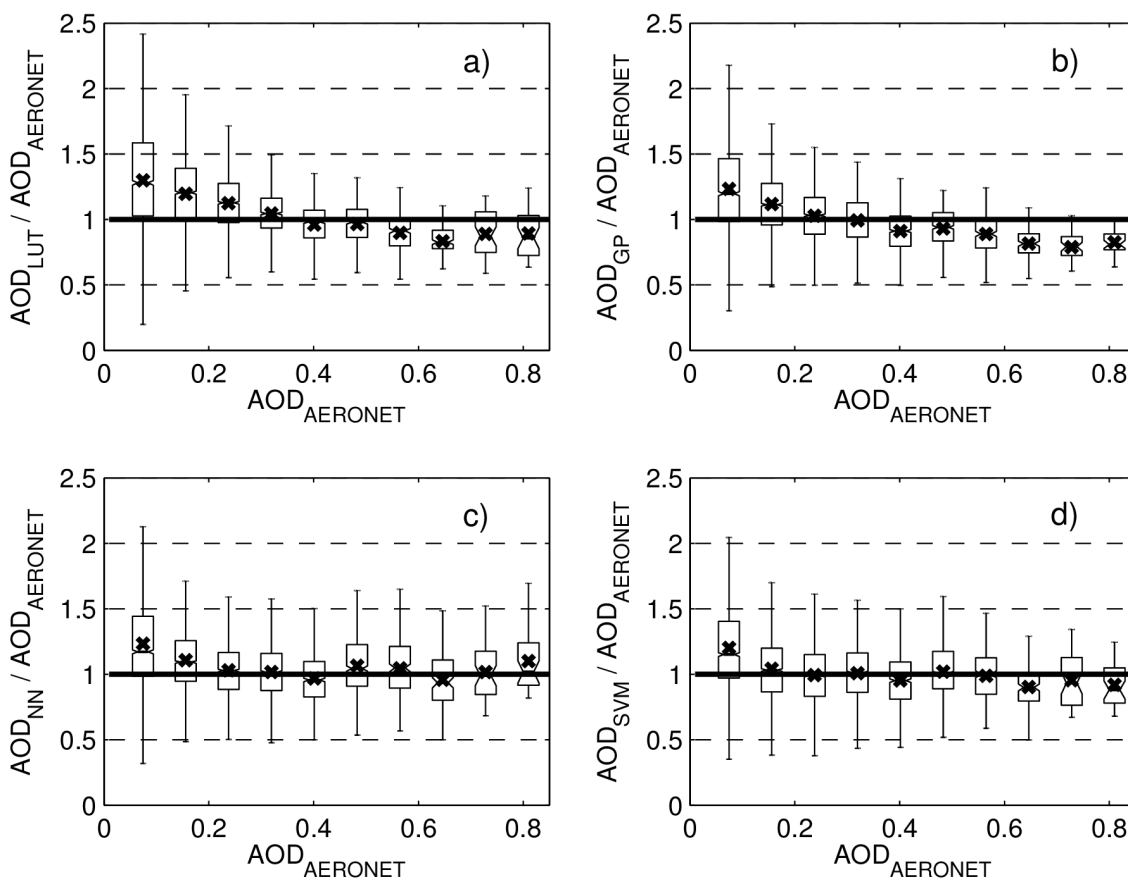


Figure 3: The same as Fig. 2, but in the vertical axis is the ratio of the predicted to the observed (AERONET) AOD.

5

10

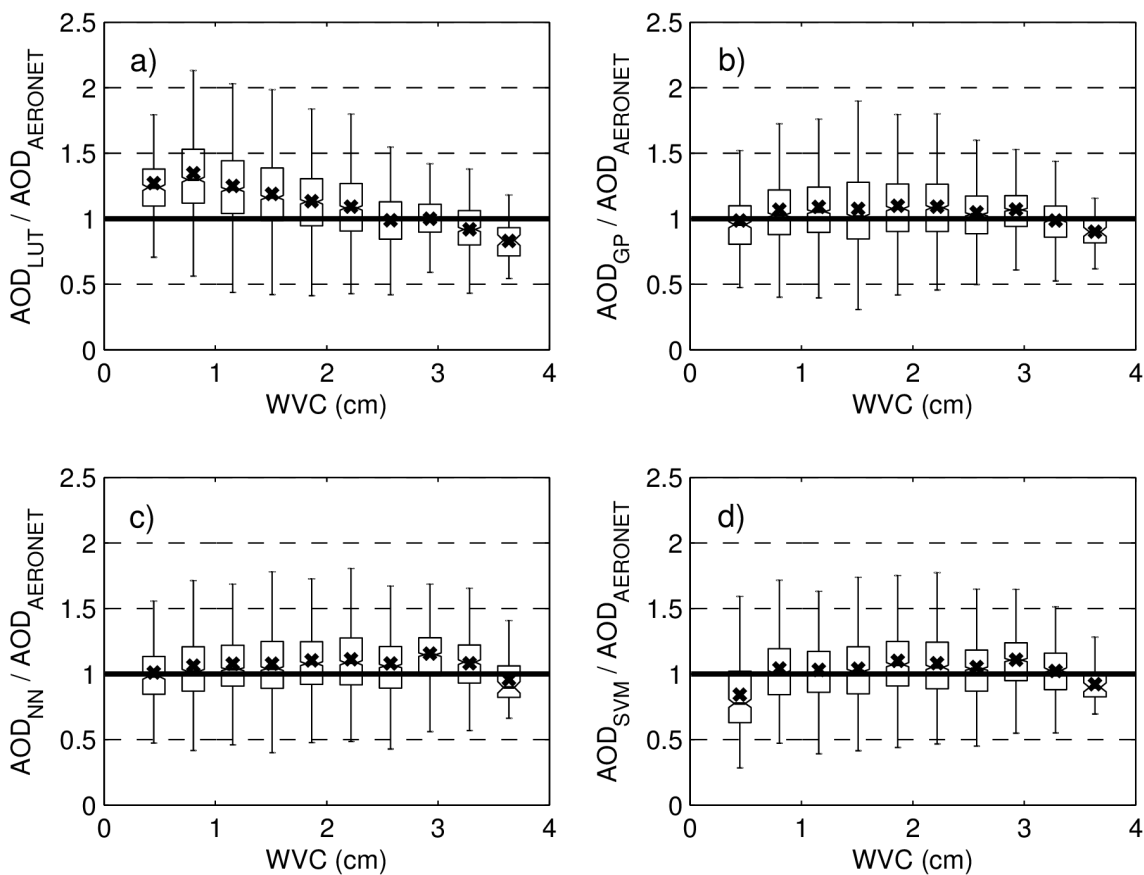


Figure 4: The same as Fig. 3, but the ratio of predicted to measured AOD is given as a function of the water vapor column (WVC).

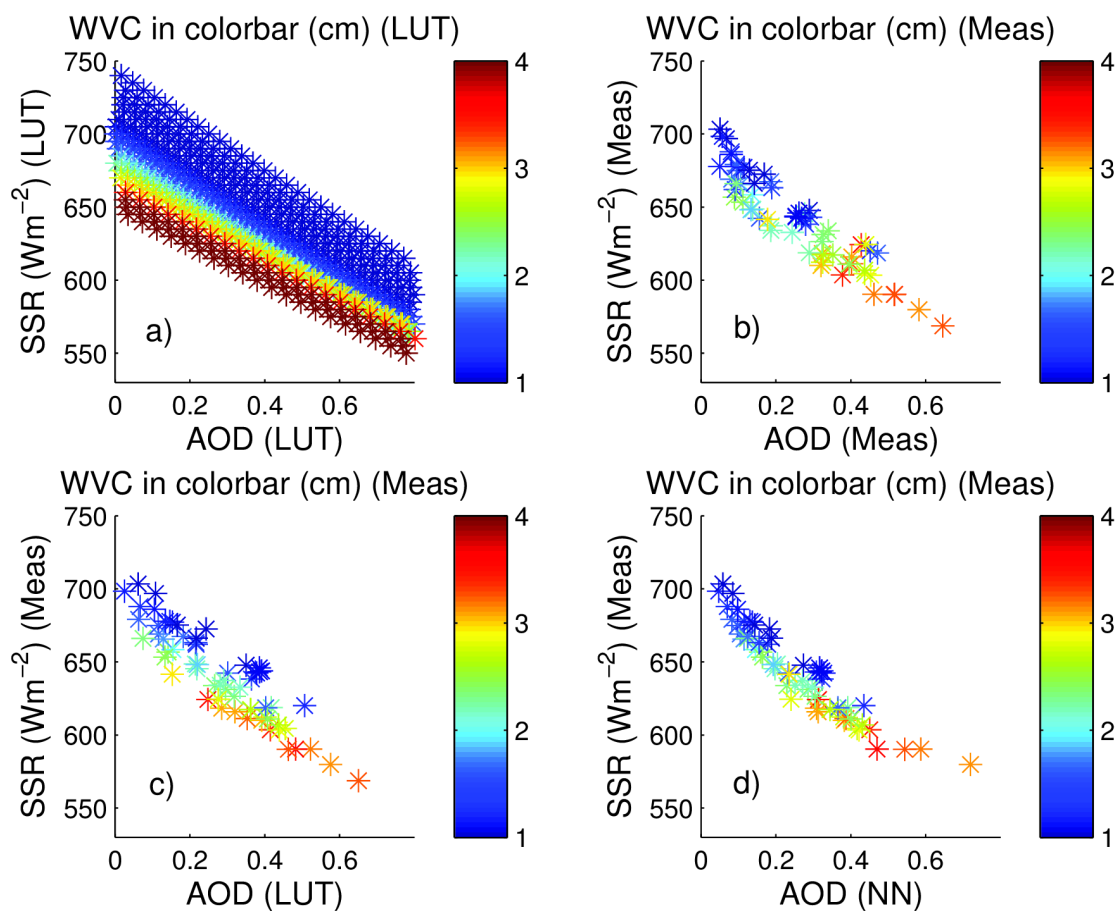


Figure 5: Solar surface radiation (SSR), aerosol optical depth (AOD) and water vapor column (WVC) for a fixed solar zenith angle (49.75° - 50.25°) for a) look-up table (LUT) and b) measurements (Meas). The predicted AODs for c) LUT and d)

5 neural network (NN) corresponding the same SSR, WVC and SZA.

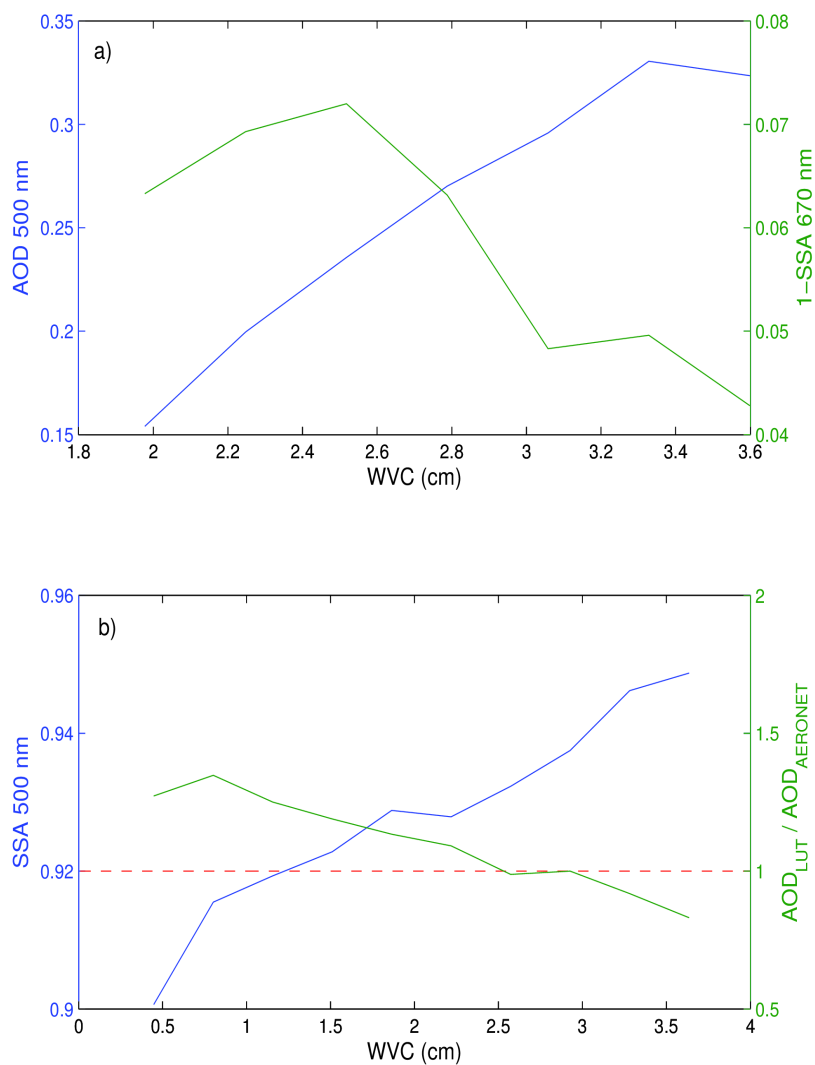


Figure 6: a) Aerosol optical depth (AOD), water vapor column (WVC) and 1-SSA at 670 nm from the AERONET inversion sky data. b) SSA at 500 nm, WVC and the LUT's predicted AOD divided with the observational AOD (AERONET), with the red line fixed to SSA (500 nm) = 0.92 (as in LUT).